Multilayer Nitroazobenzene Films Covalently Attached to Carbon. An AFM and Electrochemical Study

Paula A. Brooksby and Alison J. Downard*

MacDiarmid Institute for Advanced Materials and Nanotechnology, Department of Chemistry, University of Canterbury, Private Bag 4800, Christchurch, New Zealand

Received: August 30, 2004; In Final Form: March 6, 2005

Nitroazobenzene films have been grafted to pyrolyzed photoresist films by electrochemical reduction of the corresponding diazonium salt in acetonitrile solution. Two component films were also prepared by electrochemically grafting methylbenzene layers to preformed NAB films. Voltammetric investigation of the films in aqueous acid medium and the measurement of film thickness using atomic force microscopy (AFM) lead to new insights into film structure. In aqueous acid solution, the azobenzene groups have no detectable electroactivity and not all nitro groups in the films can be reduced. These findings point to a compact film structure in which proton diffusion is limited. There may also be spatial inhibition of the conformational changes that accompany azobenzene reduction. For increasingly thick NAB films, the peak for reduction of the nitro groups moves to more negative potentials and the peaks become more asymmetric in shape. These changes are interpreted in terms of the dielectric properties and the rate of proton diffusion in the films. Film thickness was measured by ploughing through the film with an AFM tip. When an NAB film prepared in acetonitrile solution is reduced in aqueous acid, the film thickness decreases by more than 50%. The changes can be partially reversed by treatment in acetonitrile−electrolyte solution and hence are attributed to ion−solvent induced swelling and shrinking. Thus, the large decrease in thickness detected by AFM after treatment of the film in aqueous acid is consistent with the compact film structure revealed by electrochemistry.

Introduction

Carbon materials are becoming increasingly important because their surfaces can be easily modified using electrochemical[1−3] and chemical[4] techniques. The most widely studied method for grafting an aryl (Ar) derivative directly to a carbon surface (C_s) is via reduction of the corresponding diazonium salt (eq 1). The resulting interface can exhibit desirable qualities depending on the type of chemical modifier that was used.

$$C_s + R{-}Ar{-}N_2^+ + e^- \rightarrow C_s{-}Ar{-}R + N_2 \qquad (1)$$

The problem with graphitic carbon as a substrate is its inhomogeneous surface that has randomly dispersed regions of sp^2 and sp^3 type carbon of indeterminate domain size. Most often, the covalent modification is kinetically favorable at sp^2 (or defect) sites, leaving sp^3 regions relatively unmodified. With multilayered films, we could expect a typically amorphous film structure to emerge depending on how each layer is anchored to the previous one. If each new layer results in a branching growth pattern, then the final film structure may resemble a type of polymer network. In this case, the surface structure of the carbon electrode becomes less important. If, however, the growth of the multilayer film strictly follows a particular orientation, then the resulting film structure will be influenced by the carbon surface. The superiority of one type of film compared to another depends entirely on the desired properties of the film.

Conjugated aromatic species that are covalently attached to carbon have recently become the subject of study for molecular junction applications. Investigations of a monolayer of 4-nitroazobenzene (NAB) bound to carbon suggested the phenyl ring was conjugated with the graphitic π network of the carbon substrate.[5,6] In aprotic solvent, and with an increasingly negative applied electrode potential, the electron density redistribution in the bound NAB predominantly affected the nitro group and the phenyl ring adjacent to the nitro group. However, at a sufficiently negative potential, electron transfer from carbon to NAB occurred and the resulting structure was proposed to be "quinoid" like with the NAB−carbon interface behaving as if it is one electronic system. Molecular junctions made with phenyl, biphenyl, and terphenyl species at carbon and Hg electrodes[7] alluded to a similar interfacial conjugation. However, a very different mechanism occurs in aqueous acidic solutions, where the electrochemical reduction of aromatic nitro groups gives the amine functionality with smaller amounts of hydroxylamine and nitroso groups also present because of incomplete electroreduction.[1−3,8] The film structure and electronic behavior under these conditions is not as well understood.

In addition to the nitro group, the azobenzene moiety in NAB is electroactive.[9] The voltammetry in protic and aprotic solvents, of solution-phase derivatives and species assembled on Au and conducting glass surfaces, has been documented.[10−13] In protic media, a single two-electron, two-proton reduction step produces the −NH−NH− group, which can be reoxidized back to azobenzene at relatively moderate potential. At larger negative overpotential, an additional two-electron reduction has been proposed in which the −N−N− bond cleaves thus giving two amine-terminated products.[10] For self-assembled monolayer film, the voltammetric response of azobenzene depended on the free space within the film and on the presence of small charge-compensating cations (or protons) that are proposed to act as

* To whom correspondence should be addressed. Tel: 64-3-3642501; fax: 64-3-3642110; e-mail: alison.downard@canterbury.ac.nz.

10.1021/jp046095z CCC: $30.25
Published on Web 04/06/2005

"ion-gates" for electron transfer. A compact azobenzene film in aprotic media has no significant electroactivity from the −N═N− moiety. Solvent molecules and larger cations are unable to penetrate the film, so the −N═N− group is simply acting as a molecular conductor of electrons from the metal to the outer perimeter of the film. As the porosity of the film is increased, a notable increase in the electroactivity of the −N═N− group is observed and reflects the change in accessibility of the −N═N− group.

The aqueous electrochemistry of NAB films grafted to carbon by diazonium reduction has not previously been studied in detail. The presence of the nitro and the azobenzene moieties, both with electroactivity expected to be dependent on film structure, suggests that this should be an informative system to study. In this work, NAB films were prepared by reduction of the corresponding diazonium salt in an acetonitrile solution (eq 1), and two component films were also prepared by electrochemically grafting a layer of methylbenzene groups onto an existing NAB film. The electrochemical response of the $-NO_2$ and azobenzene groups was used to assess the internal film structure, while AFM was used to profile the film heights and provide topographical information. The carbon electrode was prepared from photoresist coated onto a silicon substrate and pyrolyzed at high temperatures to give a pyrolyzed photoresist film (PPF).[14] PPF surfaces have substantially similar electrochemical behavior to glassy carbon and are versatile in that they can be made relatively easily and can provide a renewable interface that is free from introduced contaminants that often afflict other carbon surfaces (introduced from the cleaning step). Importantly, they are flat (typically less than 0.5 nm RMS roughness values) and therefore ideal for use with surface probe microscopies.

Experimental Section

Chemicals. H_2SO_4 (Aldrich) was used as received. The surface modifiers 4-(4-nitrophenylazo)benzenediazonium tetrafluoroborate ($BF_4{\cdot}N_2(C_6H_4)N_2(C_6H_4)NO_2$, NAB) and the methylbenzene ($BF_4{\cdot}N_2(C_6H_4)CH_3$, MB) diazonium salts were prepared using literature methods,[15] dried under vacuum, and stored in the dark. Acetonitrile (HPLC grade) was dried over CaH_2 for 2 days and refluxed under N_2 for 2 h prior to distilling in a N_2 atmosphere. Milli-Q water, >18 MΩ, was used for all aqueous solutions. Tetrabutylammonium tetraflouroborate ($[Bu_4N]BF_4$) was prepared by standard methods and was dried under vacuum at 80 °C for 2 days. All glassware and electrochemical cells were dried and stored at 45 °C.

PPF Preparation. Pyrolyzed photoresist film preparation followed methods described previously.[1] Briefly, a 14 mm × 14 mm Si(100) wafer substrate was twice coated with photoresist (AZ4620 (Clariant)) and then was pyrolyzed at 1050 °C for 1 h in an atmosphere of 95% nitrogen and 5% hydrogen. The furnace was stepped from room temperature to 1050 °C at an average rate of 50 °C/min. After cooling to room temperature, the pyrolyzed photoresist film (PPF) samples were removed from the furnace and stored under vacuum. Prior to use, they were briefly sonicated (3 s) in successive baths of acetone, methanol, and isopropyl alcohol and were dried with N_2. This process removed small loosely bound surface debris features. The average PPF thickness after pyrolysis was 1.5 μm, and the average sheet resistances were $1.5-4.5 \times 10^{-3}$ Ω cm and are comparable to GC substrates (4×10^{-3} Ω cm). The root-mean-squared (RMS) surface roughness of the PPF surface was determined from AFM data and was typically <0.5 nm. The RMS value was calculated over surface lengths from 2 to 10 μm depending on the scan area.

Electrochemistry. All electrochemical measurements were performed using a computer-controlled EG&G PAR model 273A instrument. The electrochemical cell has been described in full;[1] briefly, the PPF samples were mounted horizontally between an insulated metal base plate and a glass solution cell with a Viton O-ring and four springs that sealed the solution above the PPF while maintaining a copper electrical contact to the PPF external to the solution. The O-ring also defined the geometric area (0.34 cm^2) of the PPF working electrode. The secondary electrode was a Pt wire and the reference was either an SCE (for aqueous solutions) or a Ag wire pseudo-reference electrode (for acetonitrile solutions). The ferrocenium/ferrocene couple appeared at $E_{1/2} = 0.31$ V (Ag/Ag^+) in 0.1 M $[Bu_4N]BF_4$ acetonitrile solution. Solutions for electrochemistry were degassed with N_2 and all measurements were made at 22 ± 2 °C. All cyclic voltammograms were recorded with scan rate = 200 mV s^{-1}.

Surface films were prepared using controlled potential electrolysis in acetonitrile solutions containing 0.6 mM of the diazonium salt and 0.1 M $[Bu_4N]BF_4$.[1] The working electrode potential was stepped from open circuit to a potential where no electrochemical activity is recorded (0.5 V) for a time period suitable for the system to come to equilibrium. The potential was stepped from 0.5 V to the modification potential (E_{app}) for a known time, τ. For NAB films, the value of E_{app} was determined from the NAB diazonium voltammetric reduction peak potential (E_p^{red}) such that $E_{app} = E_p^{red} - 150$ mV. This potential value is sufficient to achieve reasonable modification rates without excessive overpotential. For MB films, grafting was carried out at $E_{app} = -0.6$ V with variable $\tau = 100$, 200, and 300 s. After modification, the diazonium solution was discarded, and the cell and modified PPF surface were washed with pure acetonitrile and dried with nitrogen gas. The sample was either removed for AFM analysis or additional solutions were added to the cell and electrochemistry continued. Cyclic voltammetry in aqueous acidic solutions was used to examine the redox chemistry of the NAB film. AFM was used to attain the average depth profile of the films as described previously.[1] For simplicity, all films generated on PPF surfaces from their respective diazonium salt solutions will be followed with a subscript f, (e.g., NAB_f).

Voltammetric peak analysis was performed by curve fitting the data.[16] Lorentzian, Gaussian, or mixed Lorentzian−Gaussian curves were fitted to the voltammetric peaks via the Levenberg−Marquardt algorithm. Polynomial baselines can be fit during the nonlinear least-squares iteration, or they can be solved for and subtracted from the voltammogram prior to the curvefit.

Atomic Force Microscopy. AFM (Digital Instruments Dimension 3100) topographical measurements were performed in noncontact tapping mode with a silicon cantilever (NSC 14 model, Ultrasharp) operating at moderate resonant frequencies (150−200 kHz). The images were collected with high resolution (512 samples per line) and a scan rate of 0.5 Hz. The data were collected in ambient air conditions and each scan was duplicated to ensure that any features observed were reproducible.

Film depth profiling with an AFM tip uses a technique based on mechanically removing the film from the modified PPF surface.[1] This method requires the AFM chip configuration that has three silicon cantilever tips at one end (NSC 12 model, Ultrasharp). These tips have lengths given as (D) 300, (E) 350, and (F) 250 ± 5 μm with their corresponding typical resonant frequencies at 28, 21, and 41 kHz. One of the two shorter tips located either side of the central longest tip was aligned in the usual manner for noncontact tapping mode operation. At the

same time, the AFM optical system was focused on the longest tip, which allowed for visual inspection of the surface scratching while in progress. When the shorter AFM tip approached the surface to begin a tapping mode scan, the longer tip (not in resonance) imbedded into the surface with a constant force and effectively removed the modifier from the PPF surface. The force of the imbedded tip on the surface is constant and determined by the geometry of the two tip arrangements. Use of a three-tip chip gives the choice of two forces that can be applied to the surface. The forces applied to the surface are calculated as ~0.4 μN and ~0.7 μN when using tips D and F, respectively. We determined that both forces were sufficient to scratch the PPF surface itself to an average depth of 0.3 nm. The scratch depths at bare PPF determined from both tip configurations were regularly recorded and used to adjust the measured depths of films bound to PPF.

After a set number of scans, the tips were withdrawn from the PPF surface. The sample was cleaned by sonicating in an acetone bath for a few seconds, dried with nitrogen gas, and re-imaged with the AFM using a standard noncontact tapping mode method. Loose debris from the scratch creates AFM tip−surface tracking problems and while these could be overcome by gentle air convection near the AFM tip to remove most of the debris, sample cleaning in a solvent was more effective. The accuracy of measuring a film thickness with atomic level precision was explored earlier,[1] and we have estimated that the film depths have an uncertainty associated with the bare and modified surfaces of about ±0.2 nm.

Results

The modification of carbon electrodes by electrochemical reduction of NAB diazonium salt is well documented.[1−3] Cyclic voltammograms (not shown) of 0.6 mM NAB diazonium tetrafluoroborate in 0.1 M $[Bu_4N]BF_4$ acetonitrile solution at scan rates up to 200 mV s^{-1} show an irreversible reduction peak centered near −0.05 V. The peak is due to reduction of the diazonium cation yielding an NAB radical species that covalently couples to the carbon surface. The peak is absent on the second and subsequent cycles suggesting that either NAB reduction is halted or that electron transfer through the just formed film is kinetically slow on the time scale of the voltammetry.

Electrochemistry of NAB Films. The cyclic voltammetry of NAB_f in aqueous 0.1 M H_2SO_4 is shown in Figure 1A (solid line). For comparison, the voltammogram of another surface-confined film containing the nitrophenyl group but without an azobenzene moiety (NP_f) is also shown (dotted line). NP_f was generated by reduction of 4-nitrobenzenediazonium tetrafluoroborate using similar solution conditions and electrolysis time as for NAB_f.

For both films, voltammograms were started at 0.7 V and scanned to −1.2 V for two consecutive cycles. The electrochemical responses of the films are very similar. A large reduction peak is observed at $E_{p,c}^{film} = -0.7$ V in the first cycle, but is absent in the second cycle. For NP_f, the large cathodic peak has been ascribed to reduction of the bound nitro group by the sequence of reactions shown in eqs 2 and 3,[1−3] and it is reasonable to suggest the same reaction is occurring for NAB_f.

$$-NO_2 + 4H^+ + 4e^- \rightarrow -NHOH + H_2O \qquad (2)$$

$$-NHOH + 2H^+ + 2e^- \rightarrow -NH_2 + H_2O \qquad (3)$$

On the positive potential scans, there are several small, broad oxidation peaks between 0.3 and 0.5 V, with associated

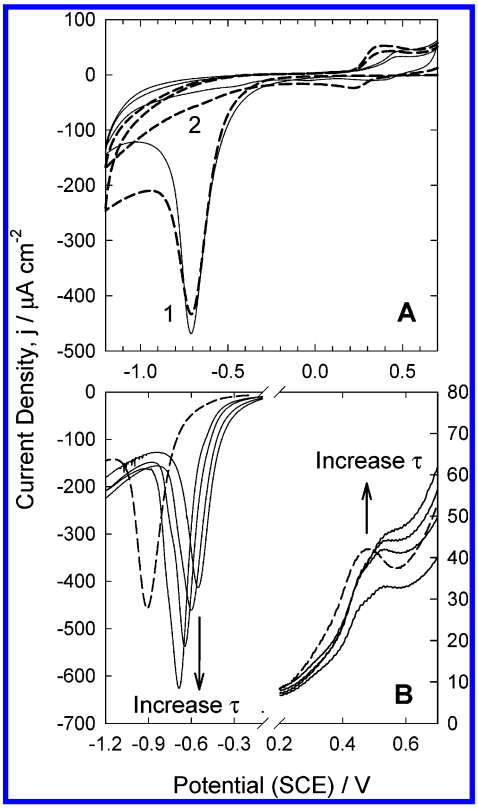

Figure 1. (A) (solid line) The cyclic voltammogram in aqueous 0.1 M H_2SO_4 of an NAB_f, scan rate = 200 mV s^{-1}. The film was generated using τ = 100 s. (dashed line) The cyclic voltammogram in aqueous 0.1 M H_2SO_4 of an NP_f on carbon, scan rate = 200 mV s^{-1}. (B) (solid line) Cyclic voltammograms of selected NAB_f surfaces illustrating peak behavior as τ increases for τ = 60, 100, 300, and 600 s. (dashed line) Cyclic voltammogram of NAB_f−MB_f for total τ = 800 s.

reduction peaks. For NP films, comparisons with the well-known electrochemistry of solution-based nitroaromatic compounds enabled these processes to be collectively assigned to the hydroxylamine/nitroso redox couple, eq 4.[1−3,17] The formation of hydroxylamine is proposed to arise from the incomplete reduction of a small fraction of nitro groups according to eq 2, that is, a 4 e^- rather than a 6 e^- reduction, and we assume that the same processes occur for NAB_f.

$$-NHOH \rightleftharpoons -NO + 2H^+ + 2e^- \qquad (4)$$

The peak potentials associated with reaction 4 for NAB_f are shifted to less positive potential compared to NP_f. The origin of the shift is unknown but may be attributed to the azobenzene influence on the phenyl ring. The similarity of the electrochemical behavior of the two films raises the question of the role of the azobenzene group in the redox chemistry of NAB_f. In aqueous 0.1 M H_2SO_4 solution, azobenzene has a chemically reversible reduction processes with $E_{1/2}$ = 0.0 V and ΔE_p = 300 mV at PPF, and for the substituted azobenzene, 4-(4-nitrophenylazo)aniline (Disperse Orange 3), the $E_{1/2}$ = 0.1 V and ΔE_p = 250 mV under the same solution conditions (not shown). These processes are assigned to the azobenzene/hydrazobenzene conversion shown in eq 5.[9]

$$-N{=}N- + 2H^+ + 2e^- \rightleftharpoons -NH{-}NH- \qquad (5)$$

Figure 1A shows no significant redox processes occurring for NAB_f close to these potentials indicating either that the peak potentials are substantially different in the film or that the

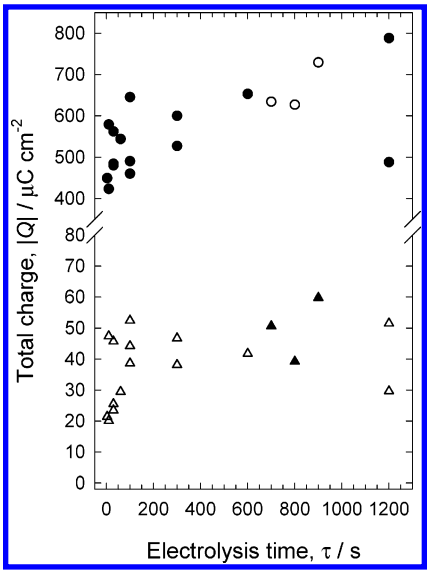

Figure 2. Graph showing the calculated total charge from voltammetric data for the reduction and oxidation peaks of NAB_f and NAB_f-MB_f films formed at various τ. (●) Total charge for $i_{p,c}^{film}$ of NAB_f; (△) total charge for $i_{p,a}^{film}$ for NAB_f; (○) total charge for $i_{p,c}^{film}$ of NAB_f-MB_f; and (▲) total charge for $i_{p,a}^{film}$ of NAB_f-MB_f.

azobenzene groups are electroinactive in these conditions. Slow electrode kinetics could lead to reduction of azobenzene to the hydrazobenzene simultaneously with reduction of the nitro groups. However, there is no evidence for oxidation of the hydrazobenzene on the return scans, and thus we conclude the azobenzene moiety is electroinactive under these conditions.

When the electrolysis time for NAB_f formation is increased, but the conditions for voltammetric examination of the films are unchanged, the voltammetric peaks behave as shown in Figure 1B (solid lines). The total charge in the reduction peak increases as expected for more electroactive material deposited at longer τ. The cathodic peak also shifts toward more negative potentials and generally begins to show some complex asymmetrical structure. Conversely, the smaller oxidation peaks, while distorted from the steeply rising background current, do not shift potential appreciably. To determine the charge associated with the reduction and oxidation processes, the peaks were curve fitted using standard fitting procedures and the sloping baseline was simulated using a Gaussian peak centered appropriately and the areas under the peaks were determined with mixed Lorentzian−Gaussian bands. The total area under the cathodic peak was calculated without regard for determining the true number of peaks present. Likewise, the total area under all of the small oxidation peaks is attributed to oxidation of hydroxylamine (eq 4). The results of the calculated total charge under these peaks are plotted against τ and are shown in Figure 2. There is a large spread to the data for short τ (<100 s), however, for larger τ the data suggest that there is a maximum charge associated with each process. Each data set was taken from a single experiment at a pristine PPF surface, so the variability of the data could in part be due to individual variations on each PPF surface influencing the total number of available attachment sites for NAB_f. Figure 3 shows the shift in the reduction peak potential for NAB_f (for the major peak in cases were a shoulder peak is also apparent) against τ, (solid symbols); these data also include a nonlinear trend line.

Electrochemistry of Two-Component NAB and MB Films. AFM thickness measurements have unequivocally demonstrated the formation of multilayered films by the diazonium reduction method.[1] Hence, it should be possible to graft a second modifier

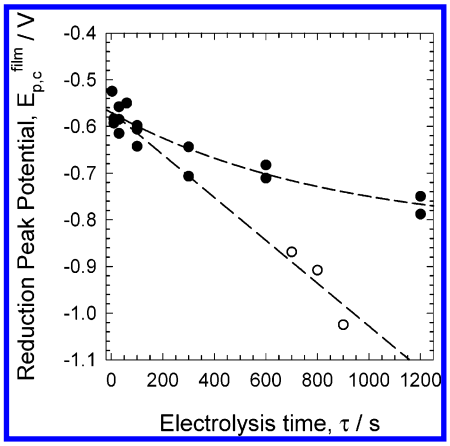

Figure 3. Graph showing the relationship between the peak reduction potential for NAB_f against electrolysis time, τ. (●) NAB_f only. (○) Dual films containing NAB_f and MB_f. The first modifier to be attached was NAB_f ($\tau_1 = 600$ s) and the second was MB_f ($\tau_2 = 100$, 200, and 300 s). The plot is given against total τ, where $\tau = \tau_1 + \tau_2$.

onto an NAB film. Initially, NAB_f was formed with τ set at 600 s in all cases. A methylbenzene (MB) film was attached to NAB_f by reduction of methylbenzenediazonium tetrafluoroborate at the NAB-modified PPF. The cyclic voltammograms of NAB_f-MB_f films in 0.1 M H_2SO_4 were substantially the same as those without MB_f except the reduction peak shifted to much more negative values, Figure 1B (dashed line). An analysis of the total charge under each of the peaks, as well as the cathodic peak shift, was performed, and the results are shown in Figures 2 and 3. Although the electrolysis time was 600 s for NAB_f formation in each of the two component films, Figures 2 and 3 show the data plotted against the cumulative time that also included the electrolysis time for MB_f.

Figure 1B shows that the NAB_f-MB_f cathodic peak has diminished peak current compared to NAB_f formed at 600 s, however, the peak width at half-height is near 10% larger. The net result is that the areas under the cathodic peaks of NAB_f (600 s), NAB_f-MB_f (600 + 100 s), NAB_f-MB_f (600 + 200 s), and NAB_f-MB_f (600 + 300 s) only vary by about 10%. Since the areas are similar for these films, the cathodic charge is also similar (Figure 2). However, Figure 3 (open circles) shows that addition of the MB_f layer shifts the NAB_f cathodic peak potential negative by up to 400 mV.

Atomic Force Microscopy. The method of depth profiling using an AFM cantilever has been described in full elsewhere.[1] Briefly, an AFM cantilever with a low resonant frequency (~40 kHz) is used to plough the surface film from the PPF substrate with a force of ~0.7 μN. This force is also sufficient to remove some of the PPF surface to an average depth of 0.3 nm, hence the film profiles presented in the figures have been adjusted by this amount. The AFM tip is not resonating while it is mechanically removing the film with an area 10 μm by 1 μm. After creating the trench, the sample was removed and briefly sonicated in acetone and then dried with compressed nitrogen to remove loose debris; although this was not always necessary, it gave better AFM tip−surface tracking interactions. With a new AFM tip, the surface was rescanned using tapping mode operation. The average cross-sectional plot of the AFM image was used to determine the depth of the film. From the cross-sectional plot, at least eight paired data points were collected where each pair contained one point from within the trench and one outside. The height differences of the film were recorded and two new random locations were selected. The estimated error in the paired data points is ±0.2 nm.

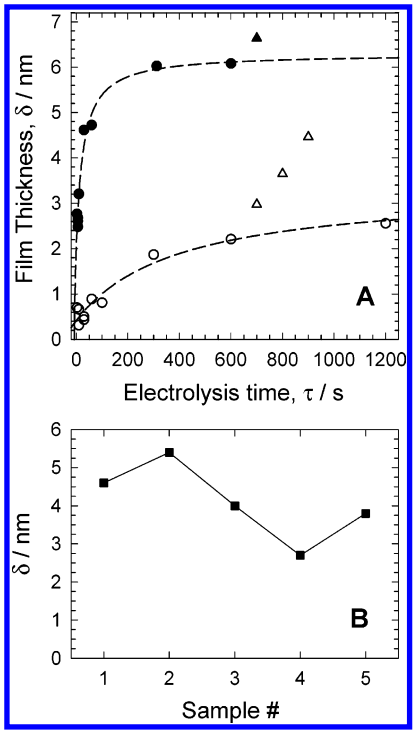

Figure 4. (A) Plot of NAB_f film thickness (δ) against formation time, τ, before and after electrochemical reduction in 0.1 M H_2SO_4. (●) δ for NAB_f before reduction; (○) δ for NAB_f after reduction; and (△) δ for NAB_f and MB_f coadsorbed films after reduction. (B) Plot of NAB_f−MB_f film thickness as a function of solvent and electrolyte conditions; Sample 1, initial film height (see text); 2, 600 s at −0.2 V in 0.1 M $[Bu_4N]BF_4$ acetonitrile; 3, 2 cycles in 0.1 M H_2SO_4 water; 4, 50 cycles in 0.1 M H_2SO_4 water; 5, 600 s at −0.2 V in 0.1 M $[Bu_4N]BF_4$ acetonitrile.

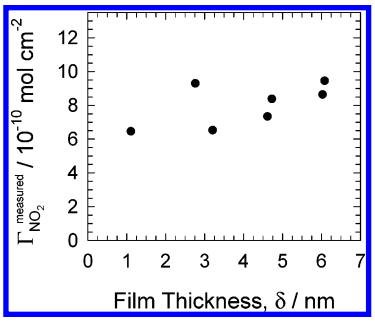

Figure 5. Plot of surface coverage of electroactive $-NO_2$ groups in NAB_f against initial film thickness, δ.

The depth profiles for films that are just formed in acetonitrile solution and those following the electrochemical reduction (of the same film) in aqueous acidic solutions are shown in Figure 4A. Data for NAB_f−MB_f surfaces are also shown, and these are plotted with a cumulative time scale for total electrolysis time. From the conditions used in this study, the thickness of the just formed NAB_f approaches a value of 6.2 ± 0.4 nm. After two potential cycles in acidic conditions, the decrease in the film thickness is significant and is more than 50% of the original film height. For the two component films, NAB_f−MB_f, the thickness is incrementally larger than for NAB_f alone. By comparison, film height changes for NP_f under similar experimental conditions decreased by only 20% (from 3.5 to 2.9 nm) after reduction in aqueous acid solution.

Figure 5 shows the relationship between surface coverage of electroactive $-NO_2$ groups and the film thickness directly after formation of NAB_f in acetonitrile solution. The surface coverage was calculated from the total charge shown in Figure 2 and by taking account of the number of electrons required for the $-NO_2$ and −NHOH redox reactions. Although there is a large scatter to the data, the plot indicates that relatively small changes in the calculated surface coverage of electroactive $-NO_2$ groups accompany comparatively large increases in the measured film thickness. This observation will be addressed in the discussion.

Additional experiments were designed to identify the cause of the film shrinkage after reduction in acidic solutions. First, the electrochemical reduction converts the bound $-NO_2$ groups to $-NH_2$ (eqs 2 and 3), or more accurately (at pH 1), $-NO_2H_2^{2+}$ and $-NH_3^+$, respectively.[9] Hence, it is possible that the measured film thickness changes arise from simple electrostatic interactions between the nitro and amine interfaces and the AFM tip. To rule out this possibility, both forms of the film were scanned with SiO_x, TiO_x, and Au tips, materials that have widely differing dielectric properties. If significant electrostatic interaction between the tip and the surface exists, the images collected over the same area for each tip will show a variation in the measured height. However, the film heights determined in this way are the same within experimental error; therefore, the electrochemically induced film thickness changes are directly related to the characteristic properties of the film and not to AFM tip-to-surface interactions.

Second, the NAB_f−MB_f generated from τ_{NAB} = 600 and τ_{MB} = 300 s (the same surface in Figure 4A) was repeatedly subjected to different conditions of solution composition and potential control, and between each step the film height was determined using AFM. This film had been reduced in aqueous acid, analyzed by AFM, and stored in the dark, in ambient conditions, for approximately 6 weeks prior to this second set of experiments. The same area of the film was profiled each time from the original trench, and the results are given in Figure 4B. Sample 1 is the film thickness after the prolonged storage time; it was unchanged from the time of the original reduction step. Sample 2 is the height of the film after immersion in 0.1 M $[Bu_4N]BF_4$ acetonitrile solution with E_{app} = −0.2 V for 600 s, thus simulating film formation conditions typically employed. The height of the film increased from 4.6 to 5.4 nm. Samples 3 and 4 were treated in 0.1 M H_2SO_4 with potential cycling of the electrode between 0.7 and −1.2 V for 2 and 50 cycles, respectively. The height of the film decreases after each of these steps to 4.0 and 2.7 nm, respectively. Sample 5 was returned to 0.1 M $[Bu_4N]BF_4$ acetonitrile solution with E_{app} = −0.2 V for 600 s, giving an increase in film height from 2.7 to 3.8 nm. These experiments were designed to reproduce the conditions relevant to the film thickness measurements, and the individual influences of solution composition and applied potential have not been specifically investigated.

The topography of a NAB_f−MB_f before and after electrochemical reduction in acidic solution was also examined using AFM. For the film shown in Figure 6, the electrolysis time for NAB was 600 s and that for MB was 100 s. These AFM images are taken in near identical areas on the surface, and the dark feature to the right in the image is the film edge of a ploughed area. The higher topography spherical features near the plough edge arise from debris buildup during the AFM tip abrasion process and are not normally found on the bulk film surface. In Figure 6B, some debris has come loose during the cleaning step and has subsequently settled on the surface, as seen in the lower right of the image. It is striking how similar the film appears before and after reduction in aqueous acid, even though the film thickness has more than halved. The position and number of surface indentations or pores (small dark circular areas) at the surface appear unchanged by the reduction step.

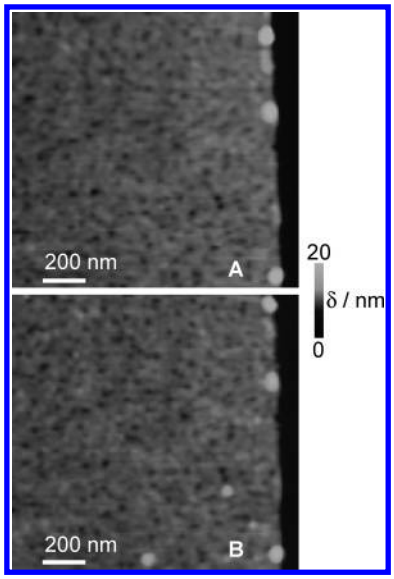

Figure 6. AFM images of the NAB_f-MB_f before and after electrochemical reduction in aqueous 0.1 M H_2SO_4 solution. The images are taken in near identical areas on the film surface. The striped feature to the right in the images is the edge of the NAB_f-MB_f film and bare PPF from the AFM depth-profiling step. (A) before and (B) after reduction. (τ_1 (NAB) = 600 s and τ_2 (MB) = 100 s).

However, after reduction there is a subtle increase in the average pore diameter concurrent with a small decrease in the distance between them. Unfortunately, the AFM resolution limit in the horizontal plane is poorer than that in the vertical plane.[1] Therefore, it is not possible to observe whether the structural changes to the film are the same in all dimensions.

Discussion

On the basis of the electrochemical and AFM results for films generated under particular conditions of solution and potential, and given the key observations that follow, an understanding of NAB film formation and structure can be described. The results indicate (i) the azobenzene group of the bound NAB film is electrochemically inactive; (ii) the addition of an MB component to the NAB film does not measurably change the number of calculated electroactive $-NO_2$ groups; (iii) the electrode potential for $-NO_2$ reduction shifts to increasingly negative values for thicker NAB films, and in the presence of MB; (iv) the measured film thickness depends on its pretreatment conditions; and (v) only small increases in the number of calculated $-NO_2$ groups accompany significant increases in measured NAB_f thickness.

NAB Film Structure. The greater thickness of films exposed to acetonitrile solutions compared with aqueous media indicates that multilayer NAB films contain a substantial amount of free space in the acetonitrile environment. We deduce that multilayer formation does not result in a significant loss of $-NO_2$ groups from the film because grafting MB_f onto NAB_f did not measurably decrease the number of accessible $-NO_2$ groups in the films. Thus, our results support the film growth mechanism proposed previously,[18] which involves attack of a solution-based radical at the positions α or β to the $-NO_2$ group of an already anchored NAB molecule. This necessarily gives a branching and porous film structure where the free space is taken up by Bu_4N^+ and BF_4^- ions and their associated acetonitrile molecules. The film under these conditions is considered swollen, but we do not know if it is maximally extended.

The possibility that loss of film material occurs when a film prepared in acetonitrile solution is reduced in aqueous acid medium cannot be discounted. However, Figure 4B shows that changes in film thickness are partially reversible indicating that the films swell after acetonitrile treatment and shrink after acid treatment. The mechanism for these processes is not clear but must be related to solvent and ion ingress and egress and associated film rearrangements. For a film treated with acetonitrile, immersion into an aqueous solution containing H^+ and SO_4^{2-} ions will create a concentration gradient within the film. At the same time, the diffusion of acetonitrile and possibly entrained Bu_4N^+ and BF_4^- out of the film will occur, also because of a concentration gradient. The process is likely hastened during potential cycling and is further influenced by changing the electrostatic and hydrophobic nature of the films through reduction of $-NO_2$ groups.[19−21] On transfer from acetonitrile to aqueous acid medium, rearrangement of the film to minimize the exposure of hydrophobic groups while maximizing the exposure to the hydrophilic $-NH_3^+$ and $-NO_2$ end groups is also expected.

In studies of self-assembled monolayers incorporating azobenzenes, the loss of azobenzene group electroactivity has been attributed to spatial inhibition of the conformation changes that accompany the azobenzene redox reaction or to slow ion transport within the layers.[11] For NAB_f in aqueous acidic solution, lack of a measurable electrochemical response from the azobenzene group confirms that the bulk film structure is sufficiently compact to bring one or both of these effects into play.

When film compaction is significant, the diffusion of protons will be a limiting process during the reduction of the $-NO_2$ groups, and the calculated number of electroactive $-NO_2$ groups in the film may be fewer than the total number present. The redox reaction is assumed to begin at the solution−film interface and moves toward the electrode rather than starting at the electrode and progressing out toward the solution. For NAB films, the $-NO_2$ groups in the outer part of the film are expected to reduce initially but the groups nearer the electrode may not be. Indeed, the relationship between surface coverage of electroactive $-NO_2$ groups and film thickness, shown in Figure 5, is consistent with only the outer $-NO_2$ groups showing electroactivity. For a fully electroactive film, a linear relationship between surface coverage and film thickness is expected, and the line of best fit should pass through the origin. The relationship was found for NP_f when film thicknesses were measured after preparation in acetonitrile and aqueous solutions.[1] For NAB_f, the lack of electroactivity of the inner $-NO_2$ groups is significant in two ways. First, it confirms the limiting ion diffusion in the films. Second, it leads to underestimation of the number of NAB groups that are bound to the surface, as determined by reduction of $-NO_2$ in aqueous acid solution. Diffusion-limited issues appear not as serious for NP_f; this may be the result of a smaller film thickness giving a shorter diffusion path length and possibly a different bulk film structure in the absence of an azobenzene group.

The addition of the MB layer to NAB_f will significantly change the dielectric and hydrophobic nature of the boundary between the bulk film and the solution. On the basis of the electrochemical response of NAB_f-MB_f, the accessibility of the $-NO_2$ group is not particularly perturbed, and grafting of MB simply increases the overall thickness of the film. However, there is a clear effect on the reduction potential peak for $-NO_2$, and this will be addressed in a following section.

Interfacial Potential Distribution. A striking feature of the NAB_f and NAB_f-MB_f electrochemistry is the sensitivity of $-NO_2$ reduction peak potential to the physical structure of the

film or the charge distribution within. There is considerable current interest in the potential distribution of the electrical double layer for surface-confined redox sites at some well-defined distance from the electrode.[22−32] A SAM containing a redox site that has uncomplicated, fast electron transfer rarely exhibits an ideal voltammetric response. More often, the voltammogram shows peak broadening, peak asymmetry, and large peak separations (>200 mV) for the reduced and oxidized forms. The models used to describe the departure from ideality are either based on a Butler−Volmer framework and the heterogeneous Marcus theory or on the interfacial potential distributions (IPD) with contributions arising from lateral interactions between adsorbates, ion-pairing, acid−base equilibrium, and dispersion of formal potentials. However, models for more complex systems such as multilayered films, irreversible electron transfer, and systems with chemical steps are not as numerously examined, or indeed absent.[27]

The Butler−Volmer and Marcus kinetic models require (in part) that adsorption follows a Langmuir isotherm that each site is equivalent and noninteracting and that the areas occupied by the reduced and oxidized species are equivalent. This model assumes the overpotential is smaller than the solvent reorganization energy. Imposing large scan rates and having small rate constants simply cause the peak potential to shift to larger overpotentials while the peak shape has a constant asymmetric appearance. Taking account of the reorganizational energy (λ), the Marcus theory predicts that as the peak potentials shift to higher overpotential, the peaks become progressively broader and the peak currents get smaller. For a decreasing λ, the voltammetric peak develops a diffusion-like tail and peak currents fall further. For very small values of λ (simulating a hydrocarbon environment), the current tail becomes very prominent and much of the total charge associated with the conversion of the surface species is contained in this region.[33]

Much of the discussion concerning the IPD model is also for monolayer systems and assumes that the redox sites are contained in one plane at some well-defined distance from the electrode and that the film is compact and impermeable to ions between the electrode and the redox site (but not necessarily between the redox site and the solution). The electrostatic potential experienced by the redox group depends on several factors: the electrode charge, the ionic strength of the solution, and the dielectric properties of the interfacial region as a whole. Hence, the voltammetric response will also depend on these factors. Further, immobilized redox centers may lead to an accumulation of discrete charges in the film as the redox reaction proceeds.[24] Hence,the potential distribution in the film, during a typical voltammetric experiment, is expected to change significantly. Recently, the IPD model was applied to a multilayered film system but with reversible electron-transfer behavior.[34] Here, the physical structure of the film allowed for interstitial ions and solvent molecules. Voltammetric peak shifts were shown to depend on the ionic concentration of the electrolyte within the film. The peaks exhibited broadening or hysteresis as the coverage of electroactive groups or the scan rate increased. These effects were discussed in terms of the ionic concentrations within the films and the subsequent modification of the IPD, as well as the hydrophilic/hydrophobic differences to the reduced/oxidized redox centers.

The models strive to describe the origin of observed peak shifts and asymmetries either in terms of kinetic parameters or the potential profile of the film, and aspects of both models could be invoked to explain the $-NO_2$ cathodic peak behavior in this case. The applied electrode potential is modified by the potential distribution across the film, which has contributions arising from the number of $-NO_2$ groups present and consequently the ionic concentration of the solution in the film. If the ionic concentration (of protons) is low, the peaks will shift to more negative potentials, and as the film thickness increases this effect becomes greater. We speculate that the diffusion of protons in the film is slow; hence, thicker films will additionally be affected during initial voltammetric conditions. For two-component films, MB_f will give a relatively hydrophobic interface between the aqueous solution and the film interior. This will slow the diffusion of aqueous phase ions across the interface and may be the origin of the large peak shifts observed for these films. Additionally, the hydrophobic MB_f layer will lower the value of λ and the dielectric constant of the film at the outer edge.

Coverage at PPF. The ion−solvent related swelling of the films must be considered when trying to determine the coverage of NAB_f or NAB_f−MB_f in terms of numbers of layers and the amount of material present. The maximum film thickness of 6.2 nm, for NAB_f pretreated in acetonitrile solution, equates to a minimum of five layers of NAB. This figure is estimated by considering a hypothetical NAB_f in which each NAB is perpendicularly bound to the preceding one. However, we cannot be sure that the film is maximally extended under these conditions. Experimental techniques that can provide molecular information about the bulk film structure are required to better estimate the true number of layers present. For now, the NAB_f structure in acetonitrile solution can be described as porous, flexible, and able to uptake ions and solvent. A more compact structure in aqueous acid solution leads to diffusion-limited electrochemical behavior. We stress that these findings pertain to NAB_f formed under the particular conditions used in this study. For different reduction overpotentials or diazonium salt concentrations, structurally different films may be produced.

Concluding Remarks

The combination of voltammetry and depth profiling using AFM is a powerful strategy for the examination of covalently attached multilayer NAB films at PPF. Smaller film heights for films treated in aqueous acid than in acetonitrile solution give direct evidence for structural changes. The nitro and azobenzene groups provide a useful means of assessing film structure. The lack of an identifiable reduction or oxidation peak originating from the azobenzene group indicates the film is relatively compact in aqueous acid solution. Under the same conditions, not all nitro groups are electroactive, consistent with the compact film structure. An important component to the electrochemical performance of the film is thus diffusion, and this is a function of the ion−solvent environment. Although charge analysis of peak areas measured from the aqueous voltammetry of an NAB film underestimates the number of bound electroactive centers, shifts in peak potentials allow for a qualitative assessment of the bulk film structure. From these results, the sensitivity of the reduction potential to the thickness and dielectric properties of the film is evident.

Acknowledgment. This work was supported by the University of Canterbury and the MacDiarmid Institute for Advanced Materials and Nanotechnology. We thank Dr. Richard Blaikie for helpful discussions on AFM imaging. P.A.B thanks Dr. John Loring for use of Linkfit curve fitting software.

References and Notes

(1) Brooksby, P. A.; Downard, A. J. *Langmuir* **2004**, *20*, 5038.
(2) Downard, A. J. *Electroanalysis* **2000**, *12*, 1085.

(3) Allongue, P.; Delamar, M.; Desbat, B.; Fagebaume, O.; Hitmi, R.; Pinson, J.; Savéant, J.-M. *J. Am. Chem. Soc.* **1997**, *119*, 201.
(4) Pandurangappa, M.; Lawrence, N. S.; Compton, R. G. *Analyst* **2002**, *127*, 1568.
(5) Itoh, T.; McCreery, R. L. *J. Am. Chem. Soc.* **2002**, *124*, 10894.
(6) Nowak, A. M.; McCreery, R. L. *Anal. Chem.* **2004**, *76*, 1089.
(7) Anariba, F.; McCreery, R. L. *J. Phys. Chem. B* **2002**, *106*, 10355.
(8) Sadler, J. L.; Bard, A. J. *J. Am. Chem. Soc.* **1968**, *90*, 1979.
(9) Smith, W. H.; Bard, A. J. *J. Am. Chem. Soc.* **1975**, *97*, 3.
(10) Yu, H.-Z.; Wang, Y.-Q.; Cheng, J.-Z.; Zhao, J.-W.; Cai, S.-M.; Inokuchi, H.; Fujishma, A.; Liu, Z.-F. *Langmuir* **1996**, *12*, 2843.
(11) Campbell, D. J.; Herr, B. R.; Hulteen, J. C.; Van Duyne, R. P.; Mirkin, C. A. *J. Am. Chem. Soc.* **1996**, *118*, 10211.
(12) Yu, H.-Z.; Ye, S.; Zhang, H.-L.; Uosaki, K.; Liu, Z.-F. *Langmuir* **2000**, *16*, 6948.
(13) Zhang, W.-W.; Li, H.-F.; Liu, L.; Xie, J.-L.; Lu, C.-S.; Zhou, Y.; Ren, X.-M.; Meng. Q.-J. *J. Colloid Interface Sci.* **2003**, *261*, 82.
(14) Ranganathan, S.; McCreery, R. L. *Anal. Chem.* **2001**, *73*, 893.
(15) Saunders: K. H.; Allen, R. L. M. *Aromatic Diazo Compounds*, 3rd ed.; Edward Arnold: London, 1985.
(16) Loring, J. S. Ph.D. Thesis, University of California at Davis, 2000.
(17) Cyr, A.; Huot, P.; Belot, G.; Lessard, J. *Electrochim. Acta* **1990**, *35*, 147.
(18) Kariuki, J. K.; McDermott, M. T. *Langmuir* **1999**, *15*, 6534.
(19) Kepley, L. J.; Bard, A. J. *J. Electrochem. Soc.* **1995**, *142*, 4129.
(20) Inzelt, G.; Bacskai, J.; Chambers, J. Q.; Day, R. W. *J. Electroanal. Chem.* **1986**, *201*, 301.
(21) Skompska, M.; Szkurlat, A.; Kowal, A.; Szklarczyk, M. *Langmuir* **2003**, *19*, 2318.
(22) Smith, C. P.; White, H. S. *Anal. Chem.* **1992**, *64*, 2398.
(23) Andreu, R.; Fawcett, W. R. *J. Phys. Chem.* **1994**, *98*, 12753.
(24) Andreu, R.; Calvente, J. J.; Fawcett, W. R.; Molero, M. *Langmuir* **1997**, *13*, 5189.
(25) Honeychurch, M. J.; Rechnitz, G. A. *Electroanalysis* **1998**, *10*, 285.
(26) Honeychurch, M. J.; Rechnitz, G. A. *Electroanalysis* **1998**, *10*, 453.
(27) Honeychurch, M. J. *Langmuir* **1998**, *14*, 6291.
(28) Deng, Z.-X.; Tong, Z.-H.; Lin, X.-Q. *J. Electroanal. Chem.* **2004**, *568*, 235.
(29) Lane, R. F.; Hubbard, A. T. *J. Phys. Chem.* **1973**, *77*, 1411.
(30) Liu, H.; Yamamoto, H.; Wei, J.; Waldeck, D. H. *Langmuir* **2003**, *19*, 2307.
(31) Ohtani, M.; Kuwabata, S.; Yoneyama, H. *Anal. Chem.* **1997**, *69*, 1045.
(32) Bard, A. J.; Faulkner, L. R. *Electrochemical Methods: Fundamentals and Applications*, 3rd ed.; John Wiley: New York, 2001.
(33) Tender, L.; Carter, M. T.; Murray, R. W. *Anal. Chem.* **1994**, *66*, 3173.
(34) Shiryaeva, I. M.; Collman, J. P.; Boulatov, R.; Sunderland, C. J. *Anal. Chem.* **2003**, *75*, 494.